J Mol Model (2013) 19:2635–2645
DOI 10.1007/s00894-013-1815-y

ORIGINAL PAPER

Molecular dynamic simulations give insight into the mechanism of binding between 2-aminothiazole inhibitors and CDK5

Wei Wang · Xiaoning Cao · Xiaolei Zhu · Yongliang Gu

Received: 11 August 2012 / Accepted: 4 March 2013 / Published online: 23 March 2013

Abstract Molecular docking, molecular dynamics (MD) simulations, and binding free energy analysis were performed to reveal differences in the binding affinities between five 2-aminothiazole inhibitors and CDK5. The hydrogen bonding and hydrophobic interactions between inhibitors and adjacent residues are analyzed and discussed. The rank of calculated binding free energies using the MM-PBSA method is consistent with experimental result. The results illustrate that hydrogen bonds with Cys83 favor inhibitor binding. The van der Waals interactions, especially the important contact with Ile10, dominate in the binding free energy and play a crucial role in distinguishing the different bioactivity of the five inhibitors.

Keywords Molecular dynamics simulation · MM-PBSA · CDK5 · 2-Aminothiazole inhibitor

Introduction

The cyclin-dependent kinases (CDKs) are catalytic units of a large family of serine/threonine kinases that control the eukaryotic cell cycle [1–5]. Most CDKs play crucial roles in apoptosis [6], the control of transcription, DNA replication, and postmitotic processes [7]. They are also considered as important targets in cancer treatment [8, 9]. It is well known that monomers of CDKs are inactive, and activation requires binding to cyclins, whose levels change during the cell cycle [10]. So far, 13 cyclin-dependent kinases (CDK1–CDK13) have been found and investigated. Among these members, CDK1, 2, 3, 4, and 6 regulate the cell cycle directly, while CDK7 controls the cycle by activating other CDKs [7, 11–14]. According to reported crystallographic structures [15], these CDKs have very similar three-dimensional (3D) structures, as reflects their high sequence similarity. Although most CDKs have been implicated in the regulation of the cell division cycle, some evidence further indicates that CDK5 is a unique member of this group [16].

CDK5 was discovered in the early 1990s. Since then, great progress has been made in identifying its functions [17]. Despite sequence identity of 60 % between CDK2 and CDK5, CDK5 is not involved in cell proliferation and its activity is restricted mainly to the central neurons system [18–21]. Moreover, there is other evidence for CDK5 activity in cellular processes such as neuronal migration, cell adhesion, and axonal transport [20, 22, 23]. CDK5 also plays an important role in learning and memory, dopamine signaling, and drug addiction [24–26]. Similar to other CDKs, monomeric CDK5 demonstrates no kinase activity and needs to bind an activating partner—p35 or p39—for its complete activation [27]. Both these non-cyclin activators of CDK5 have little sequence similarity to classical cyclins [20]. Normally, CDKs are activated in two steps [15, 28], namely, the binding of cyclins confers basal kinase activity, and phosphorylation of specific amino acids on the T-loop results in full activity. However, CDK5 is fully activated only by binding of the activating proteins p35 or p39 with the T-loop [29]. It has been shown that calcium-activated calpain cleaves p35 and p39 to p25 and p29, respectively. The cleavage of p35 to p25 by calpain under pathological conditions results in the deregulation of its activity [30, 31]. This deregulation of CDK5 has been implicated in neurodegenerative diseases such as Alzheimer's disease (AD) and Parkinson's disease, amyotrophic lateral sclerosis (ALS),

Electronic supplementary material The online version of this article (doi:10.1007/s00894-013-1815-y) contains supplementary material, which is available to authorized users.

W. Wang · X. Cao · X. Zhu (✉) · Y. Gu
State Key Laboratory of Materials-Oriented Chemical Engineering, College of Chemistry and Chemical Engineering, Nanjing University of Technology, Nanjing 210009, China
e-mail: xlzhu@njut.edu.cn

and ischemia [32–35], making CDK5/p25 (simplified hereafter as CDK5) a target for inhibitor research in neurodegenerative diseases [36].

In recent years, the design and synthesis of potent small molecule inhibitors to target CDK5 have been the topics of many important experimental studies [37–40]. For example, Daniel et al. [37] discovered a series of paullones derivatives that can inhibit various protein kinases including CDK5 in terms of the COMPARE algorithm and enzyme assay methods. Anne et al. [38] synthesized novel 5-substituted indirubins as protein kinase inhibitors, with the aim of improving their pharmacological properties. They also investigated the effect of these inhibitors on CDKs (CDK1, CDK5) and GSK-3. Mahendra et al. [39] disclosed a novel clubbed triazolyl thiazole series of CDK5 inhibitors, which are potentially useful for the treatment of Alzheimer's disease. Nassima et al. [40] synthesized 2, 6, 9-trisubstituted purines and investigated their kinase inhibitory activities and antiproliferative effects. Their results demonstrate that they exhibit potent inhibition of CDK5 and CDK1. Besides, Scott et al. [41] discovered that 4-acylamino-1, 3-thiazoles derivatives are potential CDK5 inhibitors. Recently, Christopher et al. [42] developed a series of potent and selective 2-aminothiazole inhibitors to CDK5 that are potential therapeutic agents for the treatment of Alzheimer's disease and other neurodegenerative disorders. Results suggest that slight changes of substituents or positions can significantly affect the biological activities of inhibitors. However, few related theoretical studies are reported. So far, the detailed interaction mechanisms of the inhibitors mentioned above with CDK5, which would be very important and significant for accelerating experiment studies, are not clear. Molecular dynamics (MD) simulation is a powerful tool for understanding binding mechanisms in CDK5/inhibitor complexes.

Herein, in order to obtain detailed information about the binding of inhibitors to CDK5, molecular docking, MD simulations, and binding free energy calculations were applied successfully to reveal the binding mechanism between five 2-aminothiazole inhibitors and CDK5. The major findings of this work can be summarized as follows: (1) the five 2-aminothiazole inhibitors tend to locate in the ATP-binding site; (2) hydrogen bonds and hydrophobic interactions favor the stabilization of CDK5/inhibitor binding sites; (3) the ranking of calculated binding free energies is consistent with the experimental inhibiting constants of inhibitors; and (4) the main driving force for the binding of inhibitor to CDK5 is van der Waals energy. Cys83 and Ile10 may be two key residues in distinguishing the inhibitory potency of the five inhibitors. The current work provides a better structural understanding of how inhibitors bind to CDK5 at an atomic level and will be significant for the rational design of new inhibitors to CDK5.

Computational details

Initial structure preparation

The X-ray crystal structure of CDK5 was obtained from the protein data bank (PDB code 1UNL, resolution 2.20 Å) [43]. The crystal structure of CDK5 comprises two similar sub-chains. One chain [44] was used for the molecular docking and MD simulations performed here. In this work, the five inhibitors (2-aminothiazole derivatives) were constructed by 3D graphical software, and optimized at the B3LYP/6-31G(d) level using the Gaussian 09 program [45]. The structures of the five inhibitors are shown in Fig. 1.

Molecular docking

Molecular docking was carried out by the Autodock4.0 program using the Lamarckian genetic algorithm [46]. Before docking, polar hydrogen atoms were added to CDK5 and Kollman all-atom charges were assigned to the enzyme [47]. During the docking process, CDK5 is set to be rigid while all torsional bonds of inhibitor are kept free. A total of 200 independent runs were performed with maximum of energy evaluations to 25,000,000 and a population size of 300. The grid map was centered on the ATP side of CDK5, and the three dimensions of the grid were $100\times100\times100$ points with a 0.375-Å spacing value. The structures with the lowest mean binding energy and the largest number of conformations were chosen as the preferred docking conformations.

Molecular dynamics simulation

The MD simulations were carried out using the AMBER10 software package [48]. The missing hydrogen atoms in CDK5 were added with the leap module in the AMBER10 software. The standard AMBER force field (ff03) [49] and general AMBER force field (gaff) [50] were applied to describe the potentials of proteins and ligands, respectively. The partial atomics charges on the ligands were calculated with the RESP method [51] at the B3LYP/6-31G(d) level. Counterions (Na+ ions) were added to each protein-ligand complex to neutralize the system. Each system was immersed in a truncated octahedron periodic box with TIP3P [52] water model, and the minimum distances between each complex and the box walls were taken as 10 Å. Prior to MD simulations, in order to remove conflicting contacts, energy minimizations were employed on the solvent (the complex is set to be kept fixed) and the whole system with the steepest descent method for 2,000 steps followed by the conjugated gradient method for 2,000 steps using AMBER10. After that, the position restrained dynamics simulation was performed on each system. Proteins, ligands, and water molecules were coupled separately to a temperature

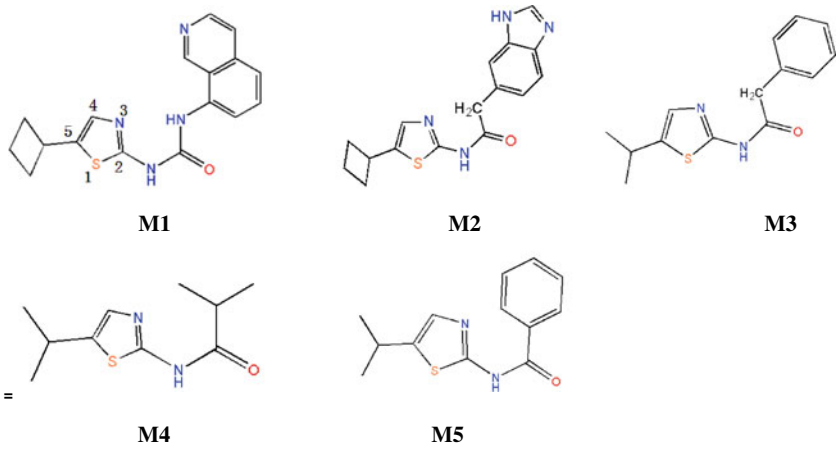

Fig. 1 Molecular structures of five 2-aminothiazole inhibitors

bath of 300 K with a coupling time of 0.1 ps. Finally, 20 ns MD simulations were carried out with the NPT ensemble. The time step was 2 fs. During the MD simulation process, the particle mesh Ewald (PME) method was applied to treat long-range electrostatic interactions [53], and all covalent bonds containing hydrogen atoms were constrained using the SHAKE algorithm [54].

Binding free energy calculation

The binding free energy and energy decomposition were analyzed by applying the molecular mechanics Poisson-Boltzmann/Generalized Born solvent accessible surface area (MM-PB/GBSA) method [55] of AMBER10. All energies were averaged for the MD trajectories. A total of 200 snapshots of the ligand, receptor, and the corresponding complex extracted from the last 10 ns of MD trajectory of the ligand–protein complex were used to estimate the binding free energies, ΔG_{bind}, based on the following equations [56, 57]:

$$\Delta G_{bind} = \Delta G(complex) - [\Delta G(protein) + \Delta G(ligand)] \quad (1)$$

$$\Delta G_{bind} = \Delta E_{gas} + \Delta G_{sol} - T\Delta S \quad (2)$$

$$\Delta E_{gas} = \Delta E_{ele} + \Delta E_{vdW} \quad (3)$$

$$\Delta G_{sol} = \Delta G_{polar} + \Delta G_{nonpolar} \quad (4)$$

$$\Delta G_{nonpolar} = \gamma(SASA) + \beta \quad (5)$$

where the gas-phase energies, ΔE_{gas}, include contributions of the van der Waals energy (ΔE_{vdw}) and the electrostatic energy (ΔE_{ele}) (Eq. 3). The solvation free energy, ΔG_{sol}, can be partitioned into two parts (Eq. 4): the polar contribution (ΔG_{polar}) and nonpolar contribution ($\Delta G_{nonpolar}$). The nonpolar contribution ($\Delta G_{nonpolar}$) to the solvation free energy was calculated from the solvent-accessible surface-area (SASA) in terms of Eq. 5. The probe radius of the solvent was set to 1.4 Å. The corresponding solvating parameters γ and β are 0.00542 kcal/(mol Å) and 0.92 kcal mol^{-1}, respectively. In our calculations, the dielectric constant was set to 1.0 for the interior solute and 80.0 for the exterior solvent. In the current work, the conformational entropy (ΔS_{bind}) [58] was neglected. If the ligands are of similar structure, the entropy contributions are not remarkably different for ligands binding to a same protein site [59]. Furthermore, the interaction energies between protein and ligand were

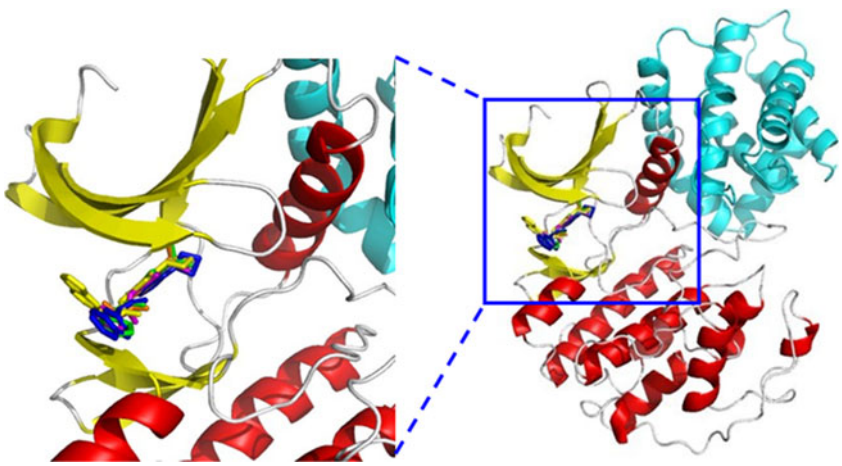

Fig. 2 Most favorable docking conformations of CDK5/inhibitor complexes (*cyan* p25). Carbon atoms of M1–M5 are colored *blue*, *yellow*, *green*, *orange*, and *magenta*, respectively

further decomposed on per residue based on the MM-GBSA method [55, 60].

Results and discussion

Five 2-aminothiazole inhibitors were docked to CDK5 and the most favorable docking structures are shown in Fig. 2. Obviously, their binding modes are similar and they locate in the ATP binding pocket, which is between the N and C terminal lobes of the kinase. The detailed binding modes for five CDK5/inhibitor complexes are represented in Fig. 3. As shown in Figs. 2 and 3, the five inhibitors position themselves inside a similar hydrophobic pocket formed by residues Ile10, Ala31, Val64, Phe80, Cys83, Phe82, Gln85, and Leu133 of CDK5, in which the substituent at the 2-position points to the solvent while the substituent at the 5-position is located in the hydrophobic pocket. Furthermore, as depicted in Fig. 3, some hydrogen bonds are established between the inhibitors and CDK5.

System stability and residue flexibility during MD simulations

In this work, 20 ns MD simulations were performed for each of the five systems. To examine the dynamic stability of the five complexes, the root-mean-squared deviations (RMSDs) relative to their starting structures of the backbone Cα atoms for the unliganded and liganded CDK5 were computed. As shown in Fig. 4, in all cases, the RMSDs increased rapidly during the first 5 ns, and became stable after ~6 ns. Thereafter, the RMSDs of the stimulated systems fluctuated

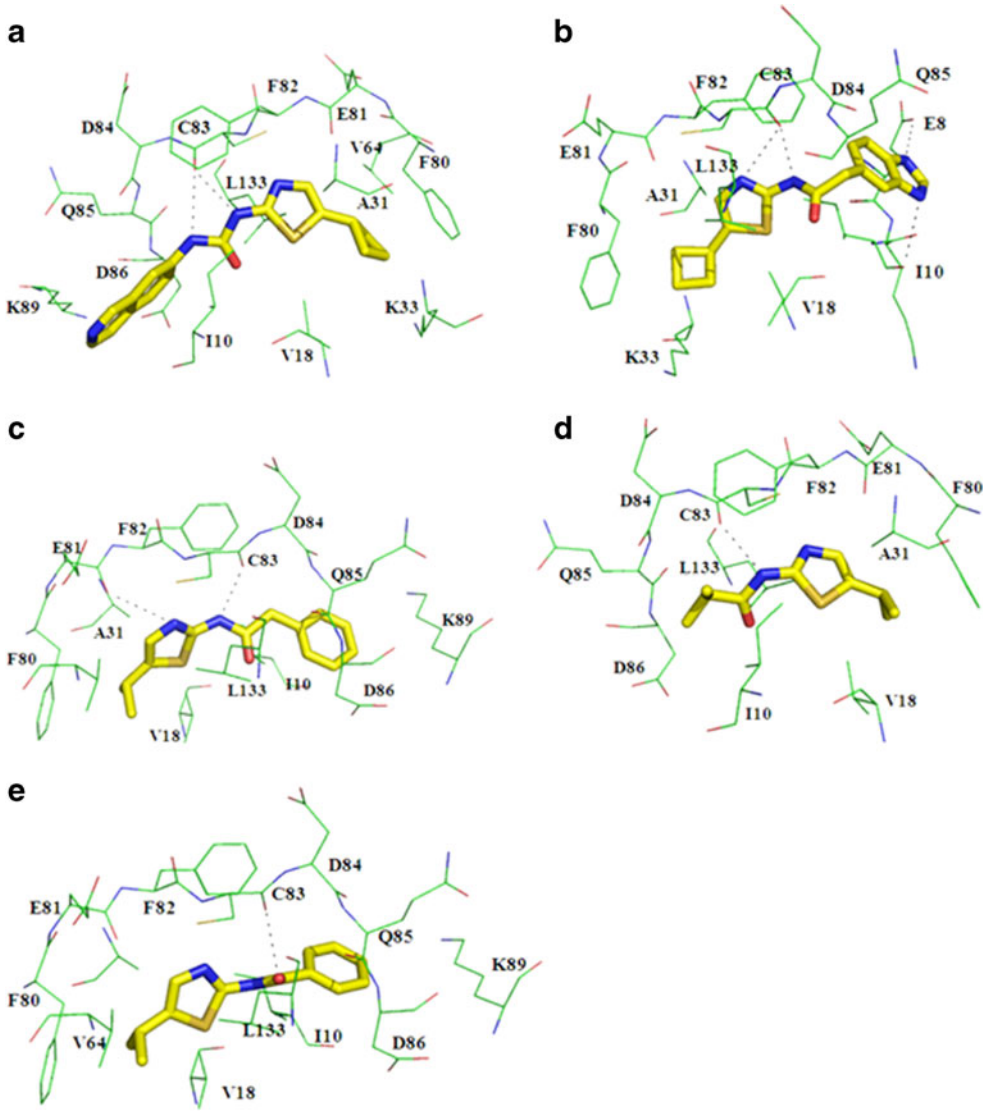

Fig. 3 Detailed binding mode of five CDK5/inhibitor complexes after molecular docking. **a** CDK5/M1, **b** CDK5/M2, **c** CDK5/M3, **d** CDK5/M4, **e** CDK5/M5. *Dotted black lines* Polar interactions or hydrogen bonds

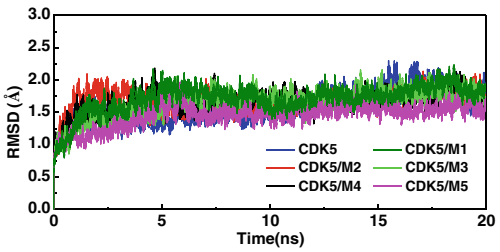

Fig. 4 Time dependence of root-mean-squared deviations (RMSDs) for five CDK5/inhibitor complexes

around ~1.5 Å, which implies that the generated MD trajectories of these complexes are stable.

It is well known that the gyration radius (Rg) is a function of molecular size [61]. The gyration radii of the unbound and bound CDK5 were computed in order to examine their sizes. As shown in Fig. 5, the average value of all complexes was 23.50±0.09 Å, which is close to that of free CDK5. The similar size of unliganded and liganded CDK5 further confirms that the structures of all complexes are stable. Furthermore, our calculated values were consistent with previous experimental values (23.60±0.08 Å) determined by X-ray diffraction [29].

The residue flexibility of bound CDK5 was examined by analyzing the root mean square fluctuation (RMSF) of the Cα atoms of each residue. Clearly, systems with the different inhibitors have similar RMSF profiles (Figs. 6 and SI-1). This is due to the fact that the binding modes between five inhibitors and CDK5 are similar overall. Moreover, for all five systems, the residues of CDK5 around the binding sites indicated by arrows in Fig. 6 and Fig. SI-1 exhibit rigid behavior [47]. However, as shown in Fig. 6, the residues with higher flexibilities distribute near the N terminal fold region (Glu25-Hie27), the PSTAIRE helix (Arg36-Gly43) and C terminal loop (Leu110-Gln130).

Binding mechanism of CDK5/inhibitor complexes and inhibitory potency of inhibitors

To understand the binding mechanism of CDK5/inhibitor complexes and the different biological activities of the five inhibitors, the program LIGPLOT[62] can be used to generate 2D schemes of protein–inhibitor complexes from MD

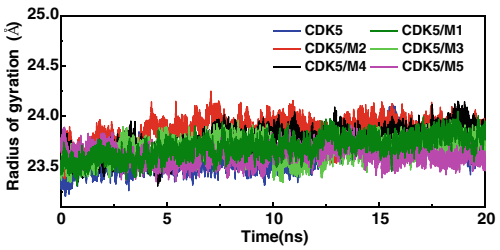

Fig. 5 Time dependence of gyration radius for bound and unbound CDK5

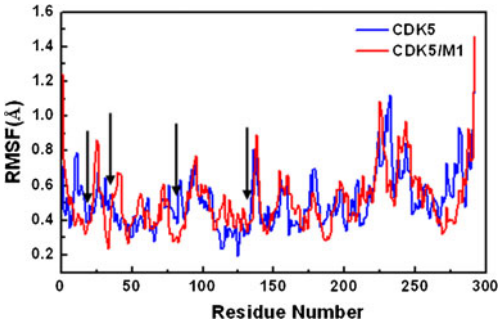

Fig. 6 Root-mean-squared fluctuations (RMSFs) of the backbone atoms versus residue number of the CDK5/M1 complex. *Arrows* Residues surrounding binding sites

simulations, and examine the hydrogen bonding and hydrophobic interactions. Figure 7a shows the interaction features and binding mode between M1 (see Fig. 1) and CDK5. As shown in Fig. 7a, three stable hydrogen bonds exist between M1 and its adjacent residues in the CDK5/M1 complex. One hydrogen bond forms between the nitrogen atom (N5) in the thiazole ring of M1 and the backbone nitrogen atom of Cys83, and the other two hydrogen bonds are established between the urea nitrogen atoms (N10 and N13) of M1 and carbonyl oxygen atom of Cys83. The distances associated with these three hydrogen bonds with time evolution are shown in Fig. 7b. Hydrogen bonds observed and their occupancies during the 20 ns simulation are displayed in Table 1. As shown in Fig. 7b and Table 1, the three hydrogen bonds are stable during the whole MD simulation, with average lengths of 0.31, 0.28, and 0.30 nm for N5(M1)-N (Cys83), N10(M1)-O(Cys83) and N13(M1)-O(Cys83), respectively. The occupancy percentages of these three hydrogen bonds are 95.97 %, 99.98 %, and 98.95 %, respectively. These stable hydrogen bonds result in stronger electrostatic interactions between M1 and CDK5. In addition, we also note that there are several hydrophobic contacts between the cyclobutyl ring/8-isoquinolyl ring of M1 and residues (Ile10, Ala31, Val64, Phe80, Asp86, Ala143). The stabilities of the hydrophobic interactions between CDK5 and M1 may be estimated by examining the time dependences of the related mass-center (CM) distances. As shown in Fig. 7c, D1 represents the distances between the 8-isoquinolyl ring of M1 and the main chain of Ile10. D2, D3, and D4 display the distances between the cyclobutyl ring of M1 and the main chains of residues (Ala31, Val64, and Phe80), respectively. The dynamic stability of the interatomic distances reveals that these hydrophobic interactions are also favorable to the stabilization of binding of M1 to CDK5. Figure 8a depicts the binding mode between the M2 and CDK5. As shown in Fig. 8a, we find that there only two stable hydrogen bonds are formed between M2 and CDK5 with the occupancy percentages of 99.62 % and 95.49 %, respectively. It is worth noting from Fig. 8a,c that residue

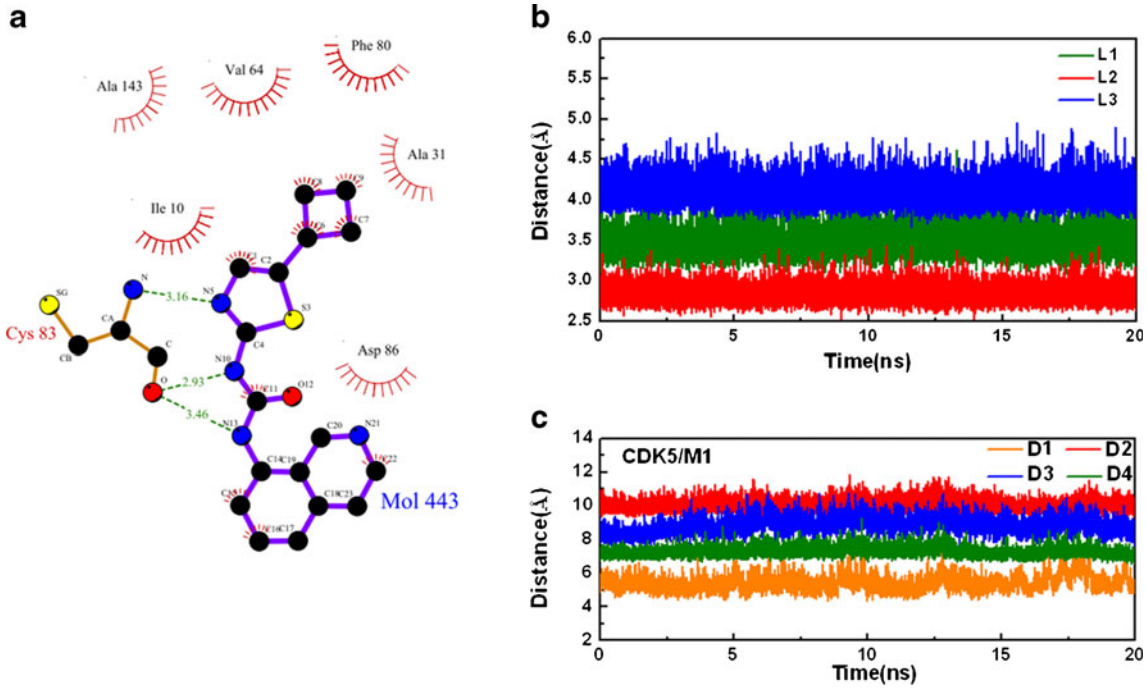

Fig. 7 **a** Two-dimensional (2D) representation of the hydrogen bond and hydrophobic interactions generated by LIGPLOT program analyses. *Dashed lines* Hydrogen bonds; *spiked residues* form hydrophobic interactions with M1. **b** Interatomic distances associated with hydrogen bond interaction of M1 in the binding site of CDK5 with time evolution. L1 and L2 represent the distances between the urea nitrogen atoms (N13 and N10) of M1 and carbonyl oxygen atom of Cys83; L3 displays the distance between the nitrogen atom (N5) at the thiazole ring of M1 and the backbone nitrogen atom of Cys83. The curves of L1 and L3 are shifted upward by 0.5 Å and 1.0 Å, respectively. **c** Mass-center distances associated with hydrophobic interactions between CDK5 and M1 at the binding site of CDK5 versus MD simulation time. The curves of D1, D2, D3 and D4 are shifted upward by 0.5, 5.0, 2.0 and 2.5 Å, respectively

Ile10 has considerable hydrophobic interaction with the substituents of M2. As shown in Fig. 8c, the stable interatomic distances related to the hydrophobic interactions for CDK5/M2 illustrate that van der Waals interactions play a dominant role in the binding of CDK5 and M2. It can be noted from Fig. SI-2 that all these 2-aminothiazole derivatives have hydrogen binding interactions with Cys83. On the other hand, there are hydrophobic interactions between the substituents at the 5-position as well as the 2-position of the thiazole ring in the inhibitors and their surrounding residues. As shown in Fig. SI-3, in the case of CDK5/M5 complex, only one hydrogen bond is formed between the nitrogen atom (N4) of the thiazole ring of M5 and the backbone nitrogen atom of Cys83, and the hydrophobic interactions between M5 and its surrounding residues are relatively weaker, which may result in a

Table 1 Hydrogen bonds formed between inhibitors and CDK5 during molecular dynamics (MD) simulations[a]

System	Donor	Acceptor	Occupancy (%)	Distance (Å)	Angle(°)
CDK5/M1	:83@O	:M1@H9-:M1@N10	99.98	2.837(0.10)	18.063(8.82)
	:83@O	:M1@H10-:83@N13	98.95	2.981(0.16)	29.80(8.57)
	:M1@N5	:83@H-:83@N	95.97	3.097(0.14)	25.39(13.19)
	:M1@O12	:11@H-:11@N	7.71	3.150(0.19)	41.10(10.81)
CDK5/M2	:83@O	:M2@H2-:M2@N6	99.62	2.945(0.14)	15.85(8.41)
	:M2@N4	:83@H-:83@N	95.49	3.120(0.14)	27.49(13.06)
CDK5/M3	:83@O	:M3@H2-:M3@N6	99.27	2.973(0.15)	15.24(8.24)
	:M3@N4	:83@H-:83@N	95.54	3.116(0.14)	27.40(13.32)
CDK5/M4	:83@O	:M4@H9-:M4@N9	96.43	2.947(0.16)	16.65(9.02)
	:M4@N4	:83@H-:83@N	92.40	3.169(0.14)	27.55(12.56)
CDK5/M5	:M5@N4	:83@H-:83@N	95.46	3.108(0.15)	25.46(12.14)

[a] Hydrogen bonds are determined by acceptor/donor atom distance of less than 3.5 Å and acceptor/H–donor angle of great than 120°

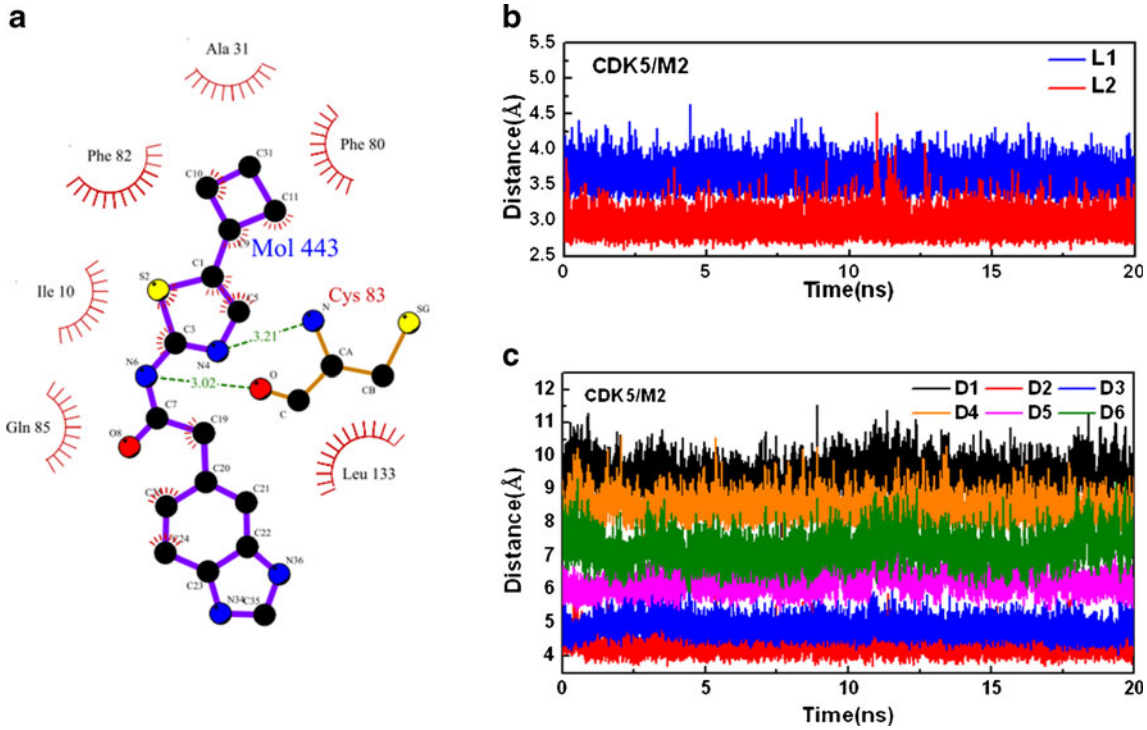

Fig. 8 **a** 2D representation of hydrogen bond and hydrophobic interactions generated by LIGPLOT program analyses. *Dashed lines* Hydrogen bonds; *spiked residues* form hydrophobic interactions with M2. **b** L1 and L2 represent the distances between atoms (N4 and N6) of M2 and nitrogen atom and carbonyl of Cys83, respectively. The curve of L1 is shifted upward with 0.5 Å. **c** Mass-center distances associated with hydrophobic interactions between CDK5 and M2 at the binding site of CDK5 versus MD simulation time. D1, D2 and D6 account for the distances between residue Ile10 and cyclobutyl ring, 5-benzimidazole group, as well as thiazole ring of M2, respectively; D3 displays the distance between the cyclobutyl group and residue Phe80; D4 depicts the distance between the 5-benzimidazole group and residue Phe82; D5 shows the distance between thiazole ring of M2 and residue Leu133. The curves of D1, D4, and D6 are shifted upward by 1.0, 1.0, and 1.0 Å, respectively

decrease in bioactivity. The results mentioned above suggest that differences in hydrogen binding and hydrophobic interactions could be major reasons for the bioactivity variance of M1(or M2) and M5.

Table 2 Binding free energy components for the protein–inhibitor complexes using the molecular mechanics Poisson-Boltzmann solvent accessible surface area (MM-PBSA) method[a]

Component[b]	CDK5/M1		CDK5/M2		CDK5/M3		CDK5/M4		CDK5/M5	
	Mean	SD[c]	Mean	SD[c]	Mean	SD[c]	Mean	SD[c]	Mean	SD[c]
ΔE_{ele}	−12.52	2.80	−12.35	3.42	−11.28	2.77	−14.90	2.23	−9.65	2.64
ΔE_{vdW}	−38.28	2.47	−37.41	2.50	−34.74	2.15	−33.27	1.96	−35.38	1.74
ΔE_{gas}	−50.81	2.99	−49.76	3.57	−46.02	3.12	−48.17	2.71	−45.04	2.74
ΔG_{pol}	27.35	3.04	28.14	4.05	25.25	2.84	28.12	2.87	27.23	3.80
$\Delta G_{nonpolar}$	−5.11	0.10	−4.92	0.12	−4.60	0.10	−4.36	0.12	−4.73	0.08
ΔG_{sol}	22.24	3.03	23.22	4.01	20.65	2.84	23.76	2.84	22.50	3.78
ΔG_{bind}	−28.56		−26.54		−25.36		−24.41		−22.53	
IC_{50} [d]	0.005		0.007		0.064		0.321		1.150	

[a] All values are given in kcal mol^{-1}

[b] Components: ΔE_{ele}: electrostatic energy in the gas phase; ΔE_{vdW}: van der Waals energy; ΔE_{gas}: total gas phase energy, which is the sum of ΔE_{ele} and ΔE_{vdW}; ΔG_{pol}: polar solvation free energy; $\Delta G_{nonpolar}$: nonpolar solvation free energy; ΔG_{sol}: sum of nonpolar and polar contributions to salvation; ΔG_{bind} : final estimated binding free energy calculated from the terms mentioned above

[c] Standard deviation of mean values

[d] All values are given in μM

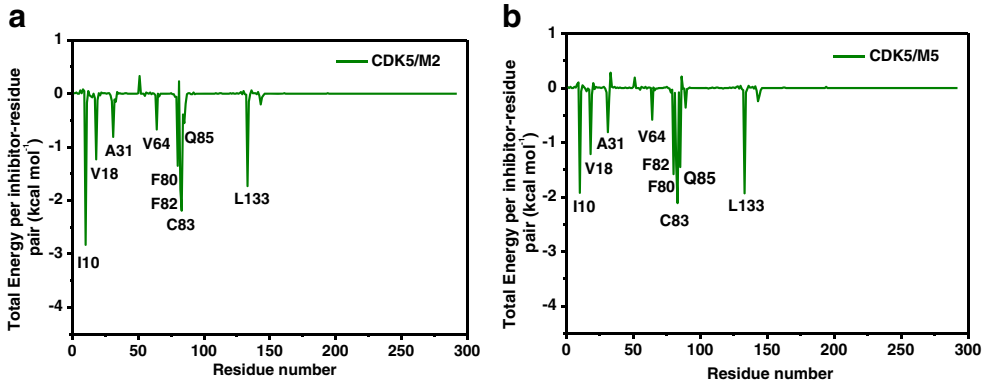

Fig. 9 Interaction spectra of inhibitor–residue pair in the protein–inhibitor complexes based on the molecular mechanics generalized Born solvent accessible surface area (MM-GB/SA) method. **a** CDK5/M2; **b** CDK5/M5

To further examine the interactions between inhibitors and CDK5, the binding free energies for five CDK5/inhibitor complexes using the MM-PBSA method were calculated as mentioned above. The results of estimated free energies and energy components of each complex are listed in Table 2. Entropy calculation is extremely time-consuming for large systems. Therefore, the entropic contribution ($T\Delta S$) to the $\Delta G_{binding}$ was not considered in current work. Estimation of energies in this manner has proven successful in previous work [63]. As shown in Table 2, the ranking of our calculated binding free energies is in approximate agreement with the experimental bioactivity data (IC_{50} values) [42]. In order to understand more deeply which energy term has more impact on the binding of CDK5/inhibitor complexes, it is necessary to compare the four individual energy components (ΔE_{ele}, ΔE_{vdW}, ΔG_{pol}, $\Delta G_{nonpolar}$). It is clear from Table 2 that the van der Waals energy term (ΔE_{vdW}) is dominant in the total binding free energy (ΔG_{bind}), revealing that the van der Waals energy term is mainly responsible for differentiating the binding affinity of five inhibitors. However, the polar solvation energy term (ΔG_{pol}) is considerably unfavorable for binding in the five complexes. The gas phase electrostatic energy term (ΔE_{ele}) makes a favorable contribution to binding, it still cannot completely cancel the negative effect caused by the polar solvation free energy (ΔG_{pol}) [64, 65]. Thus, the net electrostatic contribution ($\Delta E_{ele}+\Delta G_{pol}$) is unfavorable to the binding of the five complexes. Nonpolar solvation free energies ($\Delta G_{nonpolar}$) slightly drive the binding.

To gain insight into the difference in binding modes of the five complexes, binding free energy decomposition was performed to analyze the contribution of each residue to the binding. The total energies per inhibitor–residue pair of two complexes (CDK5/M2 and CDK5/M5 complexes) based on the MM-GB/SA method are shown in Fig. 9 (for others, see Fig. SI-4). Fig. 9a shows that the binding affinity of the potent inhibitor M2 depends mainly on residues I10, V18, F80, F82, C83, and L133, However, M5 has strong interactions with residues I10, V18, F80, F82, C83, Q85, and L133 as shown in Fig. 9b. It can be concluded from the difference of the inhibitor–residue van der Waals interaction spectra between the two inhibitors (Fig. SI-5) that residue I10 is a key residue for the different bioactivity of M2 and M5. It is worth noting from Fig. 9 and Fig. SI-4 that only nine residues (I10, V18, A31, V64, F80, F82, C83, Q85, L133) contribute significantly to total binding free energies of inhibitors with CDK5, and that

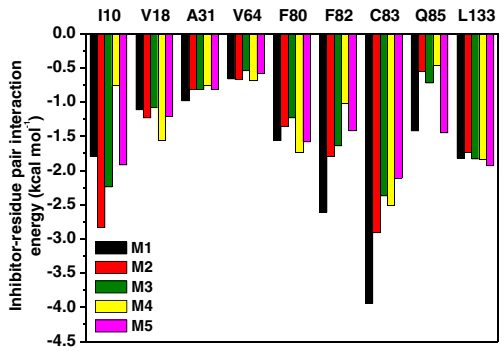

Fig. 10 Comparison of interaction energy based on the major inhibitor-residue pair in the five CDK5/inhibitor complexes using the MM-GB/SA method

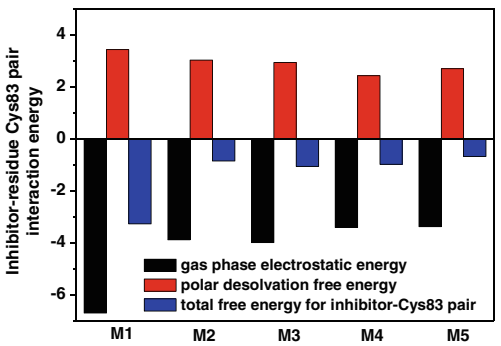

Fig. 11 Comparison of interaction energy based on the inhibitor-Cys83 pair in the five CDK5/inhibitor complexes

the contributions from other residues can be ignored, which implies that it is necessary to design new 2-aminothiazole derivatives with extended substituents to interact with those "unimportant" residues to obtain stronger binding in future studies.

To confirm the detailed binding mechanism of 2-aminothiazole inhibitors with CDK5 as mentioned above, the contributions of the major residues of each complex were compared using the MM-GB/SA method (Fig. 10). Comparison of these five systems revealed the energy differences among them. The inactive inhibitor M5 forms the same strong interactions with Ile10, Val18, Val64, Phe80, Gln85, Leu133 as inhibitor M1, but the binding contribution of M5 with residues Phe82, Cys83 tends to decrease significantly compared with inhibitor M1. For inhibitor M2, it has strong interactions with most of the same residues as inhibitor M1, weaker interactions with Phe82 and Cys83 than M1, and the strongest interaction with Ile10 compared with others. In CDK5/M1 complex, M1 has the largest electrostatic interaction with Cys83 in all systems because of the three stable hydrogen bonds established between M1 with Cys83. The energy distributions of M3 and M4 are similar except for some obvious differences in binding with residues Ile10, Val18, and Phe82. Also, the five inhibitors possess at least one stable hydrogen bond with residue Cys83. As displayed in Fig. 11, the gas phase electrostatic interactions (ΔE_{ele}) of inhibitors with the polar residue Cys83 vary greatly among the five complexes, and reveal residue Cys83 to be important for distinguishing the inhibitory potency of the five inhibitors. If we include the polar solvation contributions (ΔG_{pol}), the net electrostatic contribution ($\Delta E_{ele}+\Delta G_{pol}$) of the polar residue Cys83 in CDK5/M1 complex is favorable for the total binding free energy. However, for complexes CDK5/M2–M5, they are almost equivalent and slightly favorable to binding, which is caused by unfavorable contributions from polar solvation energies.

Conclusions

In summary, molecular docking, MD simulation, and binding free energy analysis were carried out on five CDK5/inhibitor complexes to gain some insights into the conformations and interactions for binding of the five inhibitors to CDK5. The binding free energies of the CDK5/inhibitor complexes illustrate that binding of the five inhibitors to CDK5 is energetically favored; the computed binding free energies of CDK5/inhibitor complexes are approximately consistent with the experimental inhibitory potency of the five inhibitors. Our results demonstrate that hydrogen bonds with Cys83 favor binding, and that van der Waals energy dominates in the total binding free energy. However, the polar solvation energy is considerably unfavorable for binding in the five complexes. The gas phase electrostatic energy term (ΔE_{ele}) has a positive effect on binding, but cannot completely cancel out the unfavorable contribution generated by the polar solvation free energy, i.e., the net electrostatic contribution is unfavorable to binding for the five complexes. Importantly, residues Cys83 and Ile10 are mainly responsible for distinguishing the inhibitory potency of five inhibitors. The current work may be helpful for the future design of novel CDK5 inhibitors.

Acknowledgments This work is supported by grants from the National Science Foundation of China (Nos. 21276122, 21136001, and 20876073) and Nanjing University of Technology of China (No. ZK200803).

References

1. Malumbres M, Barbacid M (2005) Mammalian cyclin-dependent kinases. Trends Biochem Sci 30:630–641
2. Gillardon F, Steinlein P, Bürger E, Hildebrandt T, Gerner C (2005) Phosphoproteome and transcriptome analysis of the neuronal response to a CDK5 inhibitor. Proteomics 5:1299–1307
3. Lees E (1995) Cyclin dependent kinase regulation. Curr Opin Cell Biol 7:773–780
4. Cardone A, Hassan SA, Albers RW, Sriram RD, Pant HC (2010) Structural and dynamic determinants of ligand binding and regulation of cyclin-dependent kinase 5 by pathological activator p25 and inhibitory peptide CIP. J Mol Biol 401:478–492
5. Ali S, Heathcote DA, Kroll SHB, Jogalekar AS, Scheiper B, Patel H, Brackow J, Siwicka A, Fuchter MJ, Periyasamy M, Tolhurst RS, Kanneganti SK, Snyder JP, Liotta DC, Aboagye EO, Barrett AGM, Coombes RC (2009) The development of a selective cyclin-dependent kinase inhibitor that shows antitumor activity. Cancer Res 69:6208–6215
6. Murray AW (2004) Recycling the cell cycle: cyclins revisited. Cell 116:221–234
7. Harper JW, Adams PD (2001) Cyclin-dependent kinases. Chem Rev 101:2511–2526
8. Feldmann G, Mishra A, Hong SM, Bisht S, Strock CJ, Ball DW, Goggins M, Maitra A, Nelkin BD (2010) Inhibiting the cyclin-dependent kinase CDK5 blocks pancreatic cancer formation and progression through the suppression of Ras-Ral Signaling. Cancer Res 70:4460–4469
9. Garrett MD, Fattaey A (1999) CDK inhibition and cancer therapy. Curr Opin Genet Dev 9:104–111
10. De Azevedo WF Jr, Mueller-Dieckmann HJ, Schulze-Gahmen U, Worland PJ, Sausville E, Kim SH (1996) Structural basis for specificity and potency of a flavonoid inhibitor of human CDK2, a cell cycle kinase. Proc Natl Acad Sci USA 93:2735–2740
11. Morgan DO (1997) Cyclin-dependent kinases: engines, clocks, and microprocessors. Annu Rev Cell Dev Biol 13:261–291
12. Hochegger H, Takeda S, Hunt T (2008) Cyclin-dependent kinases and cell-cycle transitions: does one fit all? Nat Rev Mol Cell Biol 9:910–916
13. Hengartner CJ, Myer VE, Liao SM, Wilson CJ, Koh SS, Young RA (1998) Temporal regulation of RNA polymerase II by Srb10 and Kin28 cyclin-dependent kinases. Mol Cell 2:43–53
14. Wei P, Garber ME, Fang SM, Fischer WH, Jones KA (1998) A novel CDK9-associated C-type cyclin interacts directly with HIV-1 Tat and mediates its high-affinity, loop-specific binding to TAR RNA. Cell 92:451–462
15. Jeffrey PD, Russo AA, Polyak K, Gibbs E, Hurwitz J, Massagué J, Pavletich NP (1995) Mechanism of CDK activation revealed by the structure of a cyclinA-CDK2 complex. Nature 376:313–320

16. Meyerson M, Enders GH, Wu CL, Su LK, Gorka C, Nelson C, Harlow E, Tsai LH (1992) A family of human cdc2-related protein kinases. EMBO J 11:2909–2917
17. Dhavan R, Tsai LH (2001) A decade of CDK5. Nat Rev Mol Cell Biol 2:749–759
18. Tan VBC, Zhang B, Lim KM, Tay TE (2010) Explaining the inhibition of cyclin-dependent kinase 5 by peptides derived from p25 with molecular dynamics simulations and MM-PBSA. J Mol Model 16:1–8
19. Weishaupt JH, Kussmaul L, Grötsch P, Heckel A, Rohde G, Romig H, Bähr M, Gillardon F (2003) Inhibition of CDK5 is protective in necrotic and apoptotic paradigms of neuronal cell death and prevents mitochondrial dysfunction. Mol Cell Neurosci 24:489–502
20. Dhariwala FA, Rajadhyaksha MS (2008) An unusual member of the Cdk family: Cdk5. Cell Mol Neurobiol 28:351–369
21. Smith DS, Greer PL, Tsai LH (2001) Cdk5 on the brain. Cell Growth Differ 12:277–283
22. Floyd SR, Porro EB, Slepnev VI, Ochoa GC, Tsai LH, Camilli PD (2001) Amphiphysin 1 binds the cyclin-dependent kinase (cdk) 5 regulatory subunit p35 and is phosphorylated by cdk5 and cdc2. J Biol Chem 276:8104–8110
23. Kwon YT, Tsai LH, Crandal JE (1999) Callosal axon guidance defects in $p35^{-/-}$ mice. J Comp Neurol 415:218–229
24. Smith DS, Tsai LH (2002) Cdk5 behind the wheel: a role in trafficking and transport? Trends Cell Biol 12:28–36
25. Pareek TK, Keller J, Kesavapany S, Pant HC, Iadarola MJ, Brady RO, Kulkarni AB (2006) Cyclin-dependent kinase 5 activity regulates pain signaling. Proc Natl Acad Sci USA 103:791–796
26. Lau LF, Hicks CD (2008) Cdk5 as a drug target for Alzheimer's disease. In: Ip NY, Tsai LH (eds) Cyclin dependent kinase 5 (Cdk5). Springer, New York, pp 283–299
27. Cruz JC, Tsai LH (2004) Cdk5 deregulation in the pathogenesis of Alzheimer's disease. Trends Mol Med 10:452–458
28. Russo AA, Jeffrey PD, Pavletich NP (1996) Structural basis of cyclin-dependent kinase activation by phosphorylation. Nat Struct Biol 3:696–700
29. Otyepka M, Bártová I, Kríz Z, Koca J (2006) Different mechanisms of CDK5 and CDK2 activation as revealed by CDK5/p25 and CDK2/cyclin A dynamics. J Biol Chem 281:7271–7281
30. Nath R, Davis M, Probert AW, Kupina NC, Ren X, Schielke GP, Wang KK (2000) Processing of cdk5 activator p35 to its truncated form (p25) by calpain in acutely injured neuronal Cells. Biochem Biophys Res Commun 274:16–21
31. Lee MS, Kwon YT, Li M, Peng J, Friedlander RM, Tsai LH (2000) Neurotoxicity induces cleavage of p35 to p25 by calpain. Nature 405:360–364
32. Lau LF, Ahlijanian MK (2003) Role of cdk5 in the Pathogenesis of Alzheimer's disease. Neurosignals 12:209–214
33. Smith PD, Crocker SJ, Jackson-Lewis V, Jordan-Sciutto KL, Hayley S, Mount MP, O'Hare MJ, Callaghan S, Slack RS, Przedborski S, Anisman H, Park DS (2003) Cyclin-dependent kinase 5 is a mediator of dopaminergic neuron loss in a mouse model of Parkinson's disease. Proc Natl Acad Sci USA 100:13650–13655
34. Patzke H, Tsai LH (2002) Cdk5 sinks into ALS. Trends Neurosci 25:8–10
35. Wen Y, Yang SH, Liu R, Perez EJ, Brun-Zinkernagel AM, Koulen P, Simpkins JW (2007) Cdk5 is involved in NFT-like tauopathy induced by transient cerebral ischemia in female rats. Biochim Biophys Acta 1772:473–483
36. Tarricone C, Dhavan R, Peng J, Areces LB, Tsai LH, Musacchio A (2001) Structure and regulation of the CDK5-$p25^{nck5a}$ complex. Mol Cell 8:657–669
37. Zaharevitz DW, Gussio R, Leost M, Senderowicz AM, Lahusen T, Kunick C, Meijer L, Sausville EA (1999) Discovery and initial characterization of the paullones, a novel class of small-molecule inhibitors of cyclin-dependent kinases. Cancer Res 59:2566–2569
38. Beauchard A, Ferandin Y, Frère S, Lozach O, Blairvacq M, Meijer L, Thiéry V, Besson T (2006) Synthesis of novel 5-substituted indirubins as protein kinases inhibitors. Bioorg Med Chem 14:6434–6443
39. Shiradkar MR, Akula KC, Dasari V, Baru V, Chiningiri B, Gandhi S, Kaur R (2007) Clubbed thiazoles by MAOS: a novel approach to cyclin-dependent kinase 5/p25 inhibitors as a potential treatment for Alzheimer's disease. Bioorg Med Chem 15:2601–2610
40. Oumata N, Bettayeb K, Ferandin Y, Demange L, Lopez-Giral A, Goddard ML, Myrianthopoulos V, Mikros E, Flajolet M, Greengard P, Meijer L, Galons H (2008) Roscovitine-derived, dual-specificity inhibitors of cyclin-dependent kinases and casein kinases 1. J Med Chem 51:5229–5242
41. Larsen SD, Stachew CF, Clare PM, Cubbage JW, Leach KL (2003) A catch-and-release strategy for the combinatorial synthesis of 4-acylamino-1,3-thiazoles as potential CDK5 inhibitors. Bioorg Med Chem Lett 13:3491–3495
42. Helal CJ, Sanner MA, Cooper CB, Gant T, Adam M, Lucas JC, Kang ZJ, Kupchinsky S, Ahlijanian MK, Tate B, Menniti FS, Kelly K, Peterson M (2004) Discovery and SAR of 2-aminothiazole inhibitors of cyclin-dependent kinase 5/p25 as a potential treatment for Alzheimer's disease. Bioorg Med Chem Lett 14:5521–5525
43. Mapelli M, Massimiliano L, Crovace C, Seeliger MA, Tsai LH, Meijer L, Musacchio A (2005) Mechanism of CDK5/p25 Binding by CDK inhibitors. J Med Chem 48:671–679
44. Chen Q, Cui W, Cheng YH, Zhang FS, Ji MJ (2011) Studying the mechanism that enables paullones to selectively inhibit glycogen synthase kinase 3 rather than cyclin-dependent kinase 5 by molecular dynamics simulations and free-energy calculations. J Mol Model 17:795–803
45. Frisch MJ, Trucks GW, Schlegel HB, Scuseria GE, Robb MA, Cheeseman JR, Scalmani G, Barone V, Mennucci B, Petersson GA, Nakatsuji H, Caricato M, Li X, Hratchian HP, Izmaylov AF, Bloino J, Zheng G, Sonnenberg JL, Hada M, Ehara M, Toyota K, Fukuda R, Hasegawa J, Ishida M, Nakajima T, Honda Y, Kitao O, Nakai H, Vreven T, Montgomery JA Jr, Peralta JE, Ogliaro F, Bearpark M, Heyd JJ, Brothers E, Kudin KN, Staroverov VN, Kobayashi R, Normand J, Raghavachari K, Rendell A, Burant JC, Iyengar SS, Tomasi J, Cossi M, Rega N, Millam JM, Klene M, Knox JE, Cross JB, Bakken V, Adamo C, Jaramillo J, Gomperts R, Stratmann RE, Yazyev O, Austin AJ, Cammi R, Pomelli C, Ochterski JW, Martin RL, Morokuma K, Zakrzewski VG, Voth GA, Salvador P, Dannenberg JJ, Dapprich S, Daniels AD, Farkas O, Foresman JB Ortiz JV, Cioslowski J, Fox DJ (2009) Gaussian 09 Revision.A.02. Gaussian Inc, Wallingford, CT
46. Morris GM, Goodsell DS, Halliday RS, Huey R, Hart WE, Belew RK, Olson AJ (1998) Automated docking using a Lamarckian genetic algorithnm and an empirical binding free energy function. J Comput Chem 19:1639–1662
47. Morris GM, Goodsell DS, Huey R, Olson AJ (1996) Distributed automated docking of flexible ligands to proteins parallel applications of AutoDock 2.4. J Comput Aid Mol Des 10:293–304
48. Case DA, Cheatham TA, Simmerling CL, Wang J, Duke RE, Luo R, Crowley M, Walker RC, Zhang W, Merz KM, Wang B, Hayik S, Roitberg A, Seabra G, Kolossvary I, Wong KF, Paesani F, Vanicek J, Wu X, Bronzell SR, Steinbrecher T, Gohlke H, Yang L, Tan C, Mongan J, Hornak V, Cui G, Mathews DH, Seetin MG, Sagui C, Babin V, Kollman PA (2008) AMBER 10. University of California, San Francisco, CA
49. Cornell WD, Cieplak P, Bayly CI, Gould IR, Merz KM Jr, Ferguson DM, Spellmeyer DC, Fox T, Caldwell JW, Kollman PA (1995) A second generation force field for the simulation of proteins, nucleic acids, and organic molecules. J Am Chem Soc 117:5179–5197
50. Wang J, Wolf RM, Caldwell JW, Kollman PA, Case DA (2004) Development and testing of a general Amber force field. J Comput Chem 25:1157–1174

51. Bayly CI, Cieplak P, Cornell WD, Kollman PA (1993) A well-behaved electrostatic potential based method using charge restraints for determining atom-centered charges: the RESP model. J Phys Chem 97:10269–11028
52. Jorgensen WL, Chandrasekhar J, Madura JD, Impey RW, Klein ML (1983) Comparison of simple potential functions for simulating liquid water. J Chem Phys 79:926–935
53. Darden T, York D, Pedersen L (1998) Particle mesh Ewald: an N·log(N) method for Ewald sums in large systems. J Chem Phys 98:10089–10092
54. Ryckaert JP, Ciccotti G, Berendsen HJC (1977) Numerical integration of the cartesian equations of motion of a system with constraints: molecular dynamics of *n*-alkanes. J Comput Phys 23:327–341
55. Srinivasan J, Cheatham TE, Cieplak P, Kollman PA, Case DA (1998) Continuum solvent studies of the stability of DNA, RNA, and Phosphoramidate-DNA Helices. J Am Chem Soc 120:9401–9409
56. Saíz-Urra L, Cabrera MA, Froeyen M (2011) Exploring the conformational changes of the ATP binding site of gyrase B from Escherichia colicomplexed with different established inhibitors by using molecular dynamics simulation: Protein–ligand interactions in the light of the alanine scanning and free energy decomposition methods. J Mol Graph Model 29:726–739
57. El-Barghouthi MI, Jaime C, Al-Sakhen NA, Issa AA, Abdoh AA, Al Omari MM, Badwan AA, Zughul MB (2008) Molecular dynamics simulations and MM–PBSA calculations of the cyclodextrin inclusion complexes with 1-alkanols, para-substituted phenols and substituted imidazoles. J Mol Struct (THEOCHEM) 853:45–52
58. Andricioaei I, Karplus M (2001) On the calculation of entropy from covariance matrices of the atomic fluctuations. J Chem Phys 115:6289–6292
59. Cong XJ, Tan JJ, Liu M, Chen W, Wang CX (2010) Computational study of binding mode for N-substituted Pyrrole derivatives to HIV-1 gp41. Progress Biochem Biophys 37(8):904–915
60. Kollman PA, Massova I, Reyes C, Kuhn B, Huo SH, Chong L, Lee M, Lee T, Duan Y, Wang W, Donini O, Cieplak P, Srinivasan J, Case DA, Cheatham TE (2000) Calculating structures and free energies of complex molecules: combining molecular mechanics and continuum models. Acc Chem Res 33:889–897
61. Lobanov MY, Bogatyreva NS, Galzitskaya OV (2008) Radius of gyration as an indicator of protein structure compactness. Mol Biol 42:623–628
62. Wallace AC, Laskowski RA, Thornton JM (1995) LIGPOLT: a program to generate schematic diagrams of protein-ligand interactions. Protein Eng 8:127–134
63. Lu SY, Jiang YJ, Zou JW, Wu TX (2011) Molecular modeling and molecular dynamics simulation studies of the GSK3β/ATP/Substrate complex: understanding the unique P+4 primed phosphorylation specificity for GSK3β substrates. J Chem Inf Model 51:1025–1036
64. Hu GD, Zhu T, Zhang SL, Wang D, Zhang QG (2010) Some insights into mechanism for binding and drug resistance of wild type and I50V V82A and I84V mutations in HIV-1 protease with GRL-98065 inhibitor from molecular dynamic simulations. Eur J Med Chem 45:227–235
65. Wu EL, Han K, Zhang JZ (2008) Selectivity of Neutral/Weakly basic P1 group inhibitors of thrombin and trypsin by a molecular dynamics study. Chem Eur J 14:8704–8714